

# Sequential Autonomous Exploration-Based Precise Mapping for Mobile Robots through Stepwise and Consistent Motions

Muhua Zhang, Lei Ma, Ying Wu, Kai Shen, Yongkui Sun, and Henry Leung, *Fellow, IEEE*

**Abstract**—This paper proposes a 2-D autonomous exploration and mapping framework for LiDAR-based SLAM mobile robots, designed to address the major challenges on low-cost platforms, including process instability, map drift, and increased risks of collisions and deadlocks. For frontier search, the local-global sampling architecture based on Rapidly-exploring Random Trees (RRTs) is employed. For local exploration, the proposed Self-Convergent RRT (SC-RRT) efficiently covers the reachable space within a finite time while the robot remains stationary, without relying on motion-induced sampling diversity. In addition, traversability checks during RRT expansion and global RRT pruning upon map updates eliminate unreachable frontiers, reducing potential collisions and deadlocks. For frontier point navigation, a stepwise consistent motion strategy is employed to generate motion trajectories that are more amenable to stable scan matching. The resulting straight-segment and in-place-rotation pattern improves scan-matching robustness and effectively suppresses map drift on resource-constrained platforms. For the process control, the framework serializes frontier point selection and navigation, avoiding oscillations caused by frequent goal changes in conventional parallelized processes. The waypoint retracing mechanism is incorporated to generate repeated observations, triggering loop closure detection and backend optimization in graph-based SLAM, thereby improving map consistency. Experiments in challenging simulated and real-world environments validate the effectiveness of the framework. Compared with baseline methods, the proposed framework achieves higher mapping success rates and stronger robustness on resource-constrained robots and maintains consistent mapping quality across various LiDAR field-of-view (FoV) configurations.

**Index Terms**—mobile robots, autonomous exploration, mapping, motion planning.

## I. INTRODUCTION

AUTONOMOUS collision-free exploration-based mapping enables mobile robots to navigate unknown environments and construct maps safely without human intervention. Figure 1 highlights its value for traditional LiDAR Simultaneous Localization and Mapping (SLAM)-based mobile robots [1], [2], [3], [4], as well as embodied intelligent mobile robots [5], [6], [7] which still depend on localization and path planning using grid maps. For the former, deployments often involve manual mapping performed by experienced operators. The introduction of exploration-based mapping enhances the autonomy of these robots. For the latter, advancements in autonomous exploration-based mapping enhance the robot's foundational environmental perception capabilities thereby better serving their upstream tasks. Meanwhile, high-quality maps are also crucial, especially for precise robotic operations.

This research was jointly supported by the National Natural Science Foundation of China (Grants 62203371, 61733015, U1934204). (Corresponding author: Kai Shen).

Muhua Zhang, Lei Ma, Ying Wu, Kai Shen, and Yongkui Sun are with the School of Electrical Engineering, Southwest Jiaotong University, Chengdu 611756, China (e-mail: shenkai@swjtu.edu.cn).

Henry Leung is with the Department of Electrical and Computer Engineering, University of Calgary, Calgary AB T2N 1N4, Canada (e-mail: leungh@ucalgary.ca).

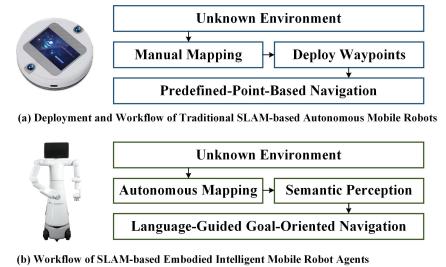
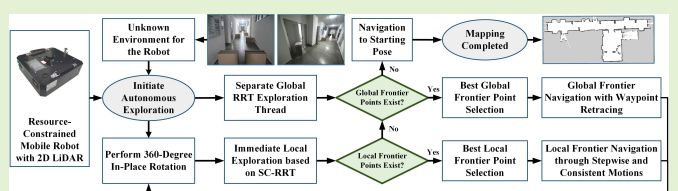


Fig. 1. Deployment and workflow of mobile robots.

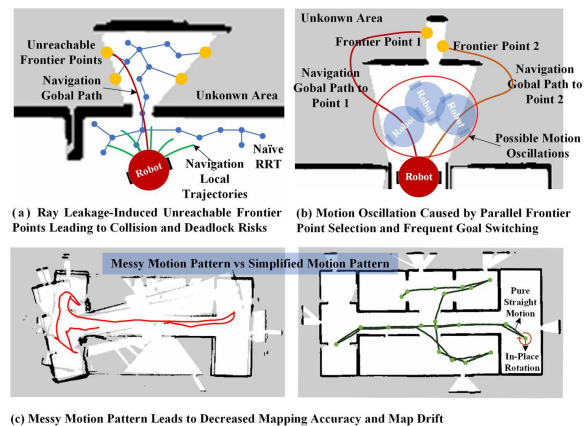


Fig. 2. Possible issues in autonomous exploration systems for mapping.

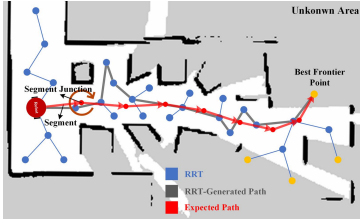


Fig. 3. Comparison of RRT-generated and expected polyline paths.

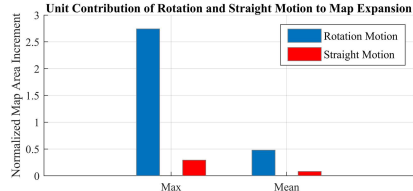


Fig. 4. Unit contribution of pure rotation and pure straight to map extension.

However, existing exploration systems still have challenges when operating in complex indoor environments and ensuring mapping precision, especially on low-cost robots, as illustrated in Figure 2. In Figure 2(a), "ray leakage" refers to appearances of areas that can be scanned by the LiDAR but remain unreachable to the robot. In such cases, naive RRT with only edge-based collision check may expand frontier points into unreachable regions. Navigating these unreachable goals may lead to potential collisions or deadlocks, obstructing the exploration process. In Figure 2(b), conventional parallel execution of frontier selection and navigation may cause frequent navigation goal switching, leading to oscillations and exploration stagnation. In Figure 2(c), several exploration systems, for example [8], [9], [10], utilize general navigation frameworks like *move\_base* [11] for moving, which generates messy motions. This results in SLAM scan matching having to estimate both rotation and translation terms simultaneously, which may introduce potential imprecisions of mapping [12], particularly on resource-constrained computing platforms or on field-of-view (FoV)-constrained LiDAR settings. In contrast, simplified and decoupled motion patterns, such as pure linear motions and in-place rotations, minimize trajectory-induced nonlinear errors. Combined with the sequential frontier search and navigation scheme, these patterns improve mapping stability and precision. The absence of the mechanism for retracing visited waypoints to generate repeated observations also limits the ability of several exploration systems to fully leverage the potential of graph-based SLAM systems such as *Cartographer* [13], [14] and *SLAM Toolbox* [15]. Moreover, their lack of a guarantee of process completeness, such as determining the completion of exploration, further constrains their practical applicability.

To address the above challenges, this paper presents an autonomous exploration framework with guaranteed process completeness and precise SLAM mapping results, which has robustness on resource-constrained low-cost mobile robots. It provides a complete closed-loop process, enabling the robot to start from a point in unknown, complex, and constrained environments, safely explore surroundings, perform precise mapping, determine completion, and autonomously return to the starting point. In this paper, precise mapping refers to constructing drift-free, mismatch-free maps that clearly

represent the environment, without guaranteeing strict metric consistency with the physical world. In these maps, robots can reliably obtain highly repeatable pose estimations at the same point, meeting the requirements of indoor mobile robot precise operations. For frontier point search, it employs the local-global sampling architecture based on multiple RRT. The Self-Convergent RRT (SC-RRT) is proposed to complete finite-time sampling of the reachable space during local exploration when the robot remains stationary, which enables the sequential decoupled exploration and navigation scheme. Traversability checks during RRT expansion and global RRT pruning upon map updates eliminate unreachable frontiers, reducing risks of collisions and deadlocks. Additionally, adaptive sampling density adjustments based on obstacle distribution enhance exploration coverage potential. For frontier point navigation, as shown in Figure 3, it employs a stepwise and consistent motion pattern to improve mapping precision. The robot follows polyline paths composed of approximately equidistant line segments, moving along each segment and performing in-place rotations at junctions to align with the next segment. Maintaining uniform segment lengths ensures consistent environmental observation. Figure 4, derived from data analysis of a real mapping process using this simplified motion pattern, shows that in-place rotations contribute more to map expansion per unit time than linear motion. Therefore, while ensuring segment length uniformity, the cumulative in-place rotation angle distance should be maximized. Figure 3 further illustrates that RRT-generated polyline paths suffer from uneven line segment lengths, penetration into narrow areas, and motion redundancy, making them unsuitable for direct use in frontier point navigations. To address these, a polyline path planner is proposed, integrating Dijkstra's algorithm as the frontend and incorporating both Bidirectional Interpolation (BI) [16], [17] and Dynamic Programming (DP) in the backend. This approach ensures segment uniformity while trying to increase the cumulative in-place rotation angle. For process control, based on SC-RRT, the framework serializes frontier point selection and navigation, preventing oscillatory behaviors caused by frequent goal switching in parallelized exploration and navigation. The visited waypoint retracing mechanism is also incorporated, enabling more repeated observations to trigger loop closure detection and backend optimization in graph-based SLAM, thereby enhancing global mapping consistency and precision.

## II. CONTRIBUTIONS

This paper presents a 2-D collision-free autonomous exploration mapping framework for low-cost mobile robots with enhanced stability and precision. Experiments conducted in both simulation and real-world scenarios validate the framework's effectiveness in autonomous exploration-based mapping and its robustness on resource-constrained robot platforms across various LiDAR FoV configurations. The key contributions of this paper are:

1) In the local-global exploration architecture based on multiple adaptive RRTs, we introduce the Self-Convergent RRT (SC-RRT) specifically for local exploration. SC-RRT achieves finite-time coverage of the reachable space while the robot remains stationary by combining batch-wise sampling with the Bidirectional Hausdorff Distance (BHD) criterion, thereby enabling a decoupled and sequential exploration and

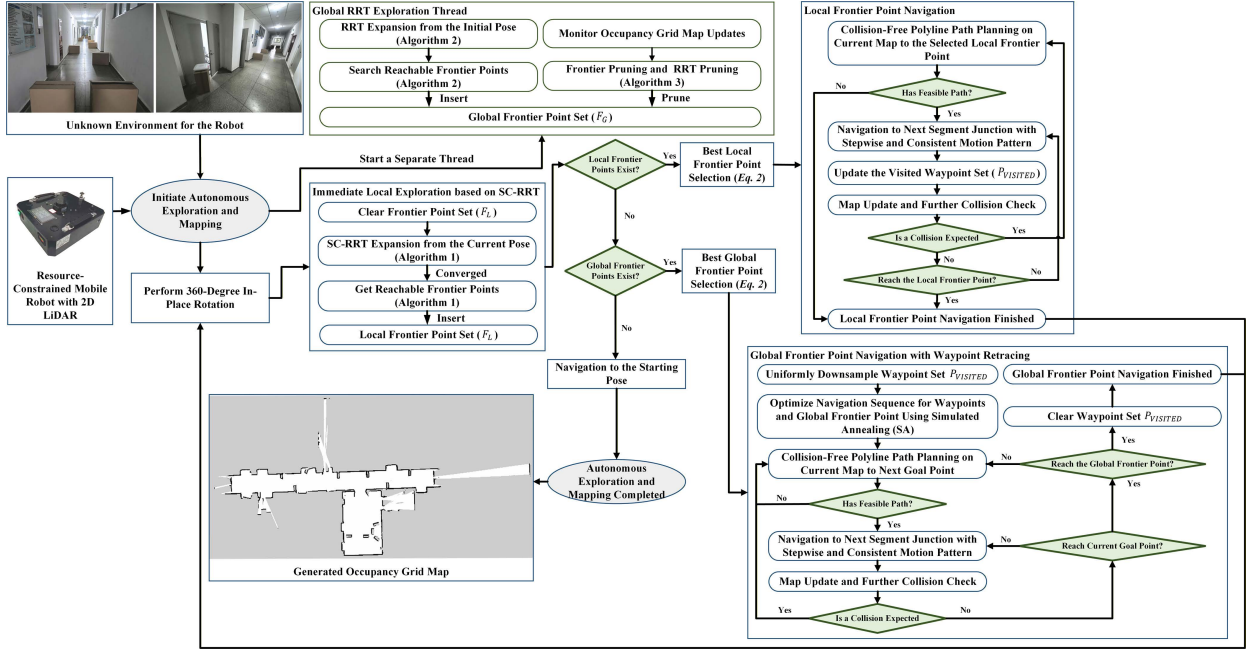


Fig. 5. The overall architecture and process design of the proposed framework.

navigation process. In addition, traversability checks during RRT expansion and global RRT pruning after map updates also ensure the validity and reachability of frontier points.

2) We employ collision-free polyline paths with uniform segment lengths to guide robot motion in exploration-based mapping and mitigate the adverse impact of irregular motion patterns on SLAM, particularly on robots constrained by computing resources and LiDAR FoV. The robot travels along straight-line segments and performs in-place rotations at junctions to align with the next segment until frontier point navigation is completed. Since in-place rotations contribute more to map expansion, the polyline should maximize cumulative rotation angles at junctions while preserving uniform segment lengths. To this end, we propose a polyline path planner that uses Dijkstra's algorithm as the frontend and incorporates Bidirectional Interpolation (BI) and Dynamic Programming (DP) as the backend.

3) The proposed framework establishes a closed-loop process from the beginning of exploration to the completion of mapping then automatically returns to the starting point. To prevent robot oscillations from frequent goal switching, execution of frontier point selection and navigation are serialized. Moreover, visited waypoint retracing is incorporated, enabling repeated generating observations to promote SLAM loop closure detection and backend optimization.

### III. RELATED WORK

#### A. Exploration in Unknown Environments

In recent years, autonomous exploration has been making continuous progress. Traditional exploration with grid map image-based frontier extraction [9], [18], [19], [20] uses computer vision algorithms to identify boundaries between known and unknown. However, these frontiers are derived purely from boundary information and do not ensure reachability. And as the map expands, computational costs increase. In contrast, RRT-based exploration [8], [10], [21], [22]

sample the space using randomly generated points, and random points in unknown areas are used as candidate frontier points, showing more advantages in efficiency, exploration coverage, and scalability. [8] and [23] propose accelerating exploration using multiple independently growing RRTs. [21] introduces a two-stage process that improves coverage through revisiting traversed areas. [10] and [22] refine RRT expansion strategies by introducing adaptive adjustment for sampling density or expansion boundary based on map data. [10] also examines the task allocation for multi-robot collaborative exploration. Additionally, various learning-based methods [24], [25], [26], [27] have been applied to autonomous exploration. However, their generalization remains challenging. For example, the model proposed in [24] is trained in office environments and may struggle to adapt to other scenarios. Overall, existing exploration research primarily focuses on efficiency and multi-robot collaboration rather than precise mapping on resource-constrained robots, often neglecting the impact of robot motion patterns. They also frequently integrate traditional SLAM methods such as gmapping [28] but lack adaptation to modern graph-based SLAM. Moreover, they rarely evaluate consistency and robustness on resource-constrained computing platforms or across diverse LiDAR FoV configurations.

#### B. Polyline Path Planning

Research on path polyline approximation, also known as path simplification, remains relatively limited. [29] proposes a key node extraction algorithm based on a divide-and-conquer approach, aiming to minimize deviations of simplified paths. OMPL [30] incorporates a path simplification algorithm that removes redundant points between two randomly selected path points within a predefined threshold window. [16] and [17] propose Bidirectional Interpolation (BI)-based path polyline approximation methods that focus on minimizing the number of segments in the path. Overall, these methods prioritize path simplification rather than guiding collision-free, stepwise, and consistent robot motions, making them unsuitable for direct

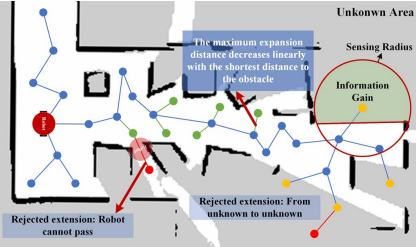


Fig. 6. RRT frontier search and information gain calculation. integration into the proposed framework.

#### IV. FRAMEWORK DESIGN

Figure 5 shows the overall architecture and process design of the proposed framework. Upon initiation, an independent global exploration thread is launched, where the global RRT expands from the starting point and continuously updates the global frontier point set  $F_G$ , compensating for potential omissions in local exploration. This thread also monitors map updates, pruning  $F_G$  and corresponding global RRT structure when certain frontier points become unreachable. The robot first conducts a stationary local frontier point search, where the local SC-RRT expands from robot's current pose to generate the local frontier point set  $F_L$ . Before each local frontier search, a 360° in-place rotation is performed to maximize the update of map known regions, improving exploration efficiency. If a feasible local frontier point is identified, the robot navigates towards it using the stepwise and consistent motion pattern until either reaching the goal or determining its infeasibility. During navigation, segment junctions visited by the robot are recorded in  $P_{VISITED}$  for subsequent waypoint retracing. This process loops between local exploration and navigation. If no local frontiers exist, the best global frontier point from  $F_G$  is selected. The robot then integrates the downsampled  $P_{VISITED}$  and optimizes the traversal sequence using Simulated Annealing (SA) before navigating with the same stepwise and consistent motion pattern. After executing the waypoint retracing mechanism, it attempts to drive the robot to navigate the selected global frontier point. If both  $F_L$  and  $F_G$  are empty, exploration is deemed complete, and the robot autonomously returns to the starting pose, finalizing the mapping process.

##### A. RRT-based Frontier Search and Pruning

The proposed framework uses SC-RRT for local frontier search and a continuous RRT with dynamic pruning for global frontier search. Both RRTs dynamically adjust the expansion step, decreasing it linearly based on the shortest distance between the node and nearby obstacles. This improves the expansion capability in narrow regions. Traversability checks are strictly applied during expansion. An expansion is discarded if any point along the candidate path is closer to an obstacle than the robot radius, which prevents the generation of unreachable frontier points. Expansions that travel through unknown regions are also removed to eliminate redundant frontiers. Finally, only nodes whose connection to their parent crosses an unknown region are considered potential frontier points. All potential frontiers are uniformly downsampled to form the final frontier point set. For proposed SC-RRT, the expansion proceeds in batches. Each batch performs sufficient node expansions to cover the explorable region under the current coverage-detection density. After each batch, the

---

##### Algorithm 1 Local SC-RRT Expansion and Frontier Search

**Input:** Initial root node  $p_{root}$ , RRT tree  $T$ , RRT sampling boundary  $B$ , grid map  $M$ , map width  $W$ , map height  $H$ , map resolution  $r_M$ , and RRT convergence density  $c_{RRT}$

1: **Output:** Frontier point set  $F$

2: **Initialize:**  $T \leftarrow \{p_{root}\}$ ,  $T_{-1} \leftarrow \emptyset$ ,  $T_{-2} \leftarrow \emptyset$ ,  $F \leftarrow \emptyset$

3:  $N_{batch} \leftarrow \lceil W \times H \times r_M^2 / \rho^2 \rceil$

4: **do**

5:   **for**  $i \leftarrow 1$  to  $N_{batch}$  **do**

6:      $p_{rand} \leftarrow \text{Random point}$

7:      $p_{nearest} \leftarrow \text{NearestNode}(p_{rand}, T)$

8:      $\eta \leftarrow \text{AdaptiveExpandDist}(p_{nearest}, M)$

9:      $p_{new} \leftarrow \text{ExtendPoint}(p_{rand}, p_{nearest}, \eta)$

10:     **if** (not  $\text{InSamplingBoundary}(p_{new}, B)$ ) or ( $p_{nearest}$  and  $p_{new}$  are both in unknown area) or (not  $\text{TraversabilityCheck}(p_{nearest}, p_{new}, M)$ ) **then**

11:       **continue**

12:     **if**  $p_{nearest}$  is in known and  $p_{new}$  is in unknown area **then**

13:        $F \leftarrow \text{UniformDownsample}(F \cup \{p_{new}\})$

14:      $T_{-2} \leftarrow T_{-1}$ ,  $T_{-1} \leftarrow T$ ,  $T \leftarrow T \cup \{p_{new}\}$

15: **return**  $F$

---

##### Algorithm 2 Global RRT Expansion and Frontier Search

**Input:** Initial root node  $p_{root}$ , RRT tree  $T$ , RRT sampling boundary  $B$ , and grid map  $M$

1: **Output:** Frontier point set  $F$

2: **Initialize:**  $T \leftarrow \{p_{root}\}$ ,  $F \leftarrow \emptyset$

3: **while** not terminated **do**

4:   **for**  $i \leftarrow 1$  to  $N_{batch}$  **do**

5:      $p_{rand} \leftarrow \text{Random point}$

6:      $p_{nearest} \leftarrow \text{NearestNode}(p_{rand}, T)$

7:      $\eta \leftarrow \text{AdaptiveExpandDist}(p_{nearest}, M)$

8:      $p_{new} \leftarrow \text{ExtendPoint}(p_{rand}, p_{nearest}, \eta)$

9:     **if** (not  $\text{InSamplingBoundary}(p_{new}, B)$ ) or ( $p_{nearest}$  and  $p_{new}$  are both in unknown area) or (not  $\text{TraversabilityCheck}(p_{nearest}, p_{new}, M)$ ) **then**

10:       **continue**

11:     **if**  $p_{nearest}$  is in known and  $p_{new}$  is in unknown area **then**

12:        $F \leftarrow \text{UniformDownsample}(F \cup \{p_{new}\})$

13:      $T \leftarrow T \cup \{p_{new}\}$

14: **return**  $F$

---

##### Algorithm 3 Global Frontier Pruning and Global RRT Pruning

**Input:** Global frontier set  $F_G$ , RRT tree  $T$ , and grid map  $M$

1: **Output:** Pruned frontier point set  $F$ , and pruned RRT tree  $T$

2: **for** each  $p_f \in F_G$  **do**

3:   **if**  $p_f$  is in known area **then**

4:     Remove  $p_f$  from  $F_G$

5:     Remove corresponding node and edge from  $T$

6:     **continue**

7:   **if**  $p_f$  is in unknown area **then**

8:      $p_{parent} \leftarrow \text{ParentNode}(p_f, T)$

9:     **while**  $\text{TraversabilityCheck}(p_f, p_{parent}, M)$  **do**

10:        $p_f \leftarrow p_{parent}$ ,  $p_{parent} \leftarrow \text{ParentNode}(p_{parent}, T)$

11:       **if**  $p_{parent}$  doesn't exist **then**

12:           **break**

13:       **if**  $p_{parent}$  exists **then**

14:           Remove  $p_f$  and all connected nodes and edges from  $T$  except  $p_{parent}$

15: **return**  $F_G, T$

---

algorithm retains the most recent three RRT trees and computes the BHD between consecutive batches. By comparing these

BHD values, the algorithm determines whether exploration has converged and autonomously terminates the process. Algorithm 1 presents the implementation of SC-RRT, and Algorithm 2 describes the RRT used for global exploration, employing the following functions:

*NearestNode*: This function receives a point  $\mathbf{p}$  and the RRT tree  $\mathbf{T}$ , returns the node in  $\mathbf{T}$  that is closest to  $\mathbf{p}$  in Euclidean distance.

*ExtendPoint*: This function receives two points  $\mathbf{p}_{rand}$  and  $\mathbf{p}_{nearest}$  and the expansion distance  $\eta$ , returns new point  $\mathbf{p}_{new}$  in the direction of  $\mathbf{p}_{rand}$  from  $\mathbf{p}_{nearest}$  with distance  $\eta$ .

*MinDistToObstacle*: This function receives a point  $\mathbf{p}$  and the grid map  $\mathbf{M}$ , returns the distance between  $\mathbf{p}$  and the nearest occupied cell on  $\mathbf{M}$  using a lookup table. The table is precomputed upon map updates, where k-d tree is utilized to determine the shortest distance from each cell to the nearest occupied cell.

*InSamplingBoundary*: This function receives a point  $\mathbf{p}$ , returns whether the point is within the RRT sampling boundary  $\mathbf{B}$ . For global exploration,  $\mathbf{B}$  is the bounding rectangle of the grid map. For local exploration,  $\mathbf{B}$  is a circle centered at the robot position  $\mathbf{p}_{robot}$  and with the sensor observation radius  $r_{sensing}$  as the radius.

*AdaptiveExpandDist*: This function receives a point  $\mathbf{p}$  and the grid map  $\mathbf{M}$ , returns the current adaptively adjusted maximum expansion distance  $\eta$  when node  $\mathbf{p}$  is the RRT parent node. Let  $d_{obs} = \text{MinDistToObstacle}(\mathbf{p}, \mathbf{M})$  and  $r_{robot}$  is the robot radius, when  $d_{obs} \geq 2r_{robot}$ ,  $\eta = \eta_{max}$ , which is the maximum expansion distance of RRT. When  $d_{obs} \leq r_{robot}$ ,  $\eta = r_{robot}$ . When  $r_{robot} \leq d_{obs} \leq 2r_{robot}$ ,  $\eta$  decreases linearly as  $d_{obs}$  decreases.

*TraversabilityCheck*: This function receives two points  $\mathbf{p}_0$  and  $\mathbf{p}_1$  and the grid map  $\mathbf{M}$ , and checks whether there is a point  $\mathbf{p}$  on the line connecting  $\mathbf{p}_0$  and  $\mathbf{p}_1$  such that  $\text{MinDistToObstacle}(\mathbf{p}, \mathbf{M}) < r_{robot}$ . If so, it returns false, and the traversability check fails.

*UniformDownsample*: This function receives point set  $\mathbf{P}$ , returns uniformly downsampled point set  $\mathbf{P}_{downsampled}$ .

*BHD*: This function receives the current RRT tree  $\mathbf{T}$  and the previous RRT tree  $\mathbf{T}_{prev}$ . It evaluates the inter tree discrepancy using the Bidirectional Hausdorff Distance (BHD). The computation can be defined as

$$\text{BHD}(\mathbf{T}, \mathbf{T}_{prev}) =$$

$$\max_{\mathbf{p} \in \mathbf{T}} \min_{\mathbf{q} \in \mathbf{T}_{prev}} \|\mathbf{p} - \mathbf{q}\|_2, \max_{\mathbf{q} \in \mathbf{T}_{prev}} \min_{\mathbf{p} \in \mathbf{T}} \|\mathbf{p} - \mathbf{q}\|_2. \quad (1)$$

This bidirectional form is equivalent to the symmetric Hausdorff distance and reflects the maximum coverage discrepancy between two consecutive batches.

As the global exploration RRT continuously samples and expands, some global frontier points may become explored or unreachable as the map updates. This results in invalid frontier points and unreachable nodes and edges within the global RRT. Therefore, upon each map update, global frontier pruning and RRT pruning are performed. Algorithm 3 shows the details of the pruning process, which utilizes the following function:

*ParentNode*: This function receives a RRT node  $\mathbf{p}$  and the RRT tree  $\mathbf{T}$ , returns the parent node of  $\mathbf{p}$  in  $\mathbf{T}$ .

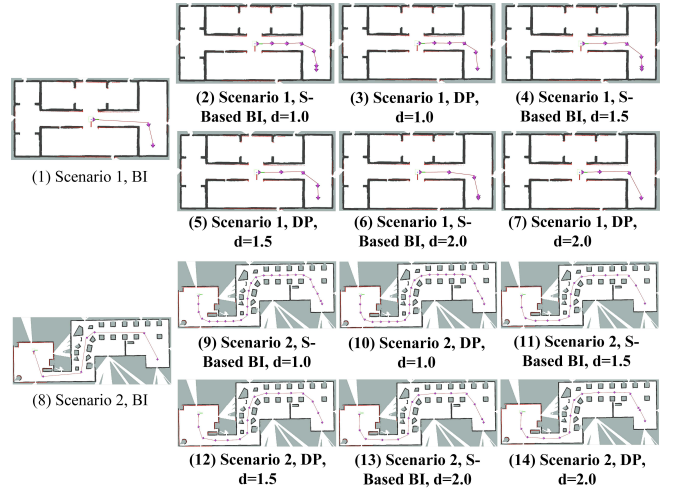


Fig. 7. Partial experimental results of the polyline path planner.

### B. Frontier Point Selection

The process of selecting the best frontier point  $\mathbf{f}_{best}$  for exploration can be expressed as

$$\begin{aligned} \mathbf{f}_{best} = \operatorname{argmax}_{\mathbf{f} \in \mathbf{F}} & (w_{info} \cdot \text{InfoGain}(\mathbf{f}) + \\ & w_{dir} \cdot (\pi - |\text{DirDiff}(\mathbf{p}_{last}, \mathbf{p}_{robot}, \mathbf{f})|) + \\ & w_{dist} \cdot \|\mathbf{p}_{robot} - \mathbf{f}\|_2 + \\ & w_{free} \cdot \text{MinDistToObstacle}(\mathbf{f}, \mathbf{M})), \end{aligned} \quad (2)$$

where  $\mathbf{F}$  is the local or global frontier point set.  $w_{info}$ ,  $w_{dir}$ ,  $w_{dist}$  and  $w_{free}$  are information gain coefficient, direction keeping coefficient, distance coefficient and area openness coefficient.  $\mathbf{p}_{last}$  is the last visited segment junction of the robot.  $\mathbf{p}_{robot}$  is the current position of the robot.  $\text{InfoGain}(\mathbf{f})$  is the area of the unknown region in  $\mathbf{M}$  covered by a circle with  $\mathbf{f}$  as the center and  $r_{sensing}$  as the radius, as shown in Figure 6.  $\text{DirDiff}(\mathbf{p}_0, \mathbf{p}_1, \mathbf{p}_2)$  is the normalized angle between the line segment from  $\mathbf{p}_0$  to  $\mathbf{p}_1$  and the line segment from  $\mathbf{p}_1$  to  $\mathbf{p}_2$ . This evaluation function prioritizes frontier points that are farther from the robot, aligned with the direction of the robot's trajectory, located in more open spaces, and contain a greater potential for expansion, thereby balancing efficiency, continuity, and safety.

### C. Frontier Point Navigation

For frontier point navigation, the robot follows a stepwise and consistent motion pattern guided by polyline global paths. These paths should maintain uniform segment lengths while maximizing the cumulative robot in-place rotation at segment junctions. Rotations are used to align with the direction of the next segment. Once polyline global paths are generated, motion planner controls the velocity to perform high-precision straight line tracking along each segment and rotations in place at the junctions. For motion planning, this work adopts the method from [2], while for polyline path planning, we propose an approach that integrates Dijkstra's algorithm as the frontend and incorporates Bidirectional Interpolation (BI) and Dynamic Programming (DP) as the backend. The BI-based and DP-based post-processing approaches are independent, allowing either to be selected. Their respective performances will be evaluated in subsequent sections.

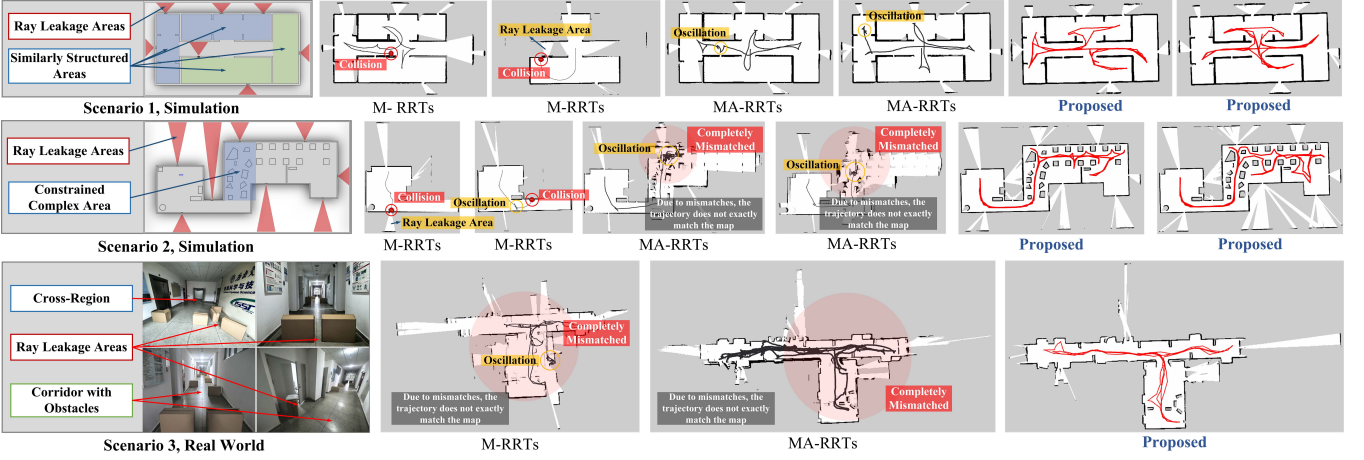


Fig. 8. Partial results of exploration-based mapping comparison experiments.

TABLE I  
EVALUATION OF POLYLINE PATHS

SCN	<i>d</i>	S-based BI			DP		
		<i>s<sub>p</sub></i>	$\varphi_{avg}^{sum}$	$t_{avg}^{calc}$	<i>s<sub>p</sub></i>	$\varphi_{avg}^{sum}$	$t_{avg}^{calc}$
1	<b>1.0</b>	0.35m	1.58	<b>0.05s</b>	<b>0.22m</b>	<b>1.65</b>	0.16s
	<b>1.5</b>	0.48m	1.34	<b>0.09s</b>	<b>0.34m</b>	<b>1.54</b>	0.22s
	<b>2.0</b>	0.57m	1.11	<b>0.12s</b>	<b>0.38m</b>	<b>1.36</b>	0.32s
2	<b>1.0</b>	0.08m	6.20	<b>0.17s</b>	<b>0.06m</b>	<b>6.52</b>	0.53s
	<b>1.5</b>	0.26m	5.71	<b>0.27s</b>	<b>0.11m</b>	<b>6.03</b>	0.76s
	<b>2.0</b>	0.50m	5.67	<b>0.36s</b>	<b>0.47m</b>	<b>5.88</b>	1.05s

TABLE II  
EVALUATION OF EXPLORATION MAPPING APPROACHES

SCN	M-RRTs			MA-RRTs			Proposed		
	CO	OS	FIN	CO	OS	FIN	CO	OS	FIN
1	8	6	6	4	6	10	<b>0</b>	<b>0</b>	<b>20</b>
2	16	4	0	5	14	1	<b>1</b>	<b>0</b>	<b>19</b>
3	7	12	1	3	13	4	<b>0</b>	<b>0</b>	<b>20</b>

Let  $\mathcal{X}$  denote the initial path generated by the Dijkstra's algorithm frontend. For  $\mathbf{x}_i \in \mathcal{X}$ , to evaluate the suitability of the exist segment from  $\mathbf{x}_{prev} \in \mathcal{X}$  to  $\mathbf{x}_i$  combined with the segment from  $\mathbf{x}_i$  to  $\mathbf{x}_{next} \in \mathcal{X}$  to be extended for the post-processing objective, we define the evaluation function  $S(\mathbf{x}_{prev}, \mathbf{x}_i, \mathbf{x}_{next})$ , which can be expressed as

$$S = k_{rot} \cdot |DirDiff(\mathbf{x}_{prev}, \mathbf{x}_i, \mathbf{x}_{next})| -$$

$$k_{uni} \cdot \|\|\mathbf{x}_{next} - \mathbf{x}_i\|_2 - d\|, \quad (3)$$

where  $k_{rot}$  and  $k_{uni}$  are the rotation angle coefficient and length deviation penalty factor, and  $d$  is the longest length of each line segment. For BI-based method, building upon [16] and [17], we refine its *Procedure for Reduce Vertices* by using  $d$  as the search window and *TraversabilityCheck* as the collision detection method, and selecting the next anchor point in a greedy manner to maximize  $S$  rather than maximizing segment length. In bidirectional path selection, the reduction direction is determined by maximizing the sum of  $S$  at all segment junctions rather than minimizing the number of segments. For DP-based post-processing, given an initial path  $\mathcal{X} = \{\mathbf{x}_0, \mathbf{x}_1, \dots, \mathbf{x}_n\}$ , the goal is to determine a subset  $\mathcal{X}' = \{\mathbf{x}_0, \mathbf{x}_{i_1}, \mathbf{x}_{i_2}, \dots, \mathbf{x}_m\}$  that maximizes  $\sum_{i=1}^{m-1} S(\mathbf{x}_{i-1}, \mathbf{x}_i, \mathbf{x}_{i+1})$ . The points in  $\mathcal{X}'$  must also satisfy  $\forall k \in \{1, \dots, m\}, \|\mathbf{x}_{i_k} - \mathbf{x}_{i_{k-1}}\|_2 \leq d$  and *TraversabilityCheck*( $\mathbf{x}_{i_{k-1}}, \mathbf{x}_{i_k}, \mathbf{M}$ ) is true. The DP formulation recursively determines the optimal path selection using the recurrence relation, can be expressed as

$$DP(i, j) = \max_{k < i} [DP(k, i) + S(\mathbf{x}_k, \mathbf{x}_i, \mathbf{x}_j)], \quad (4)$$

where  $DP(i, j)$  denotes the optimal cumulative evaluation function value for a path ending at  $\mathbf{x}_j$ , with  $\mathbf{x}_i$  as its preceding point. The final polyline path  $\mathcal{X}'$  is obtained through a retracing procedure. The last selected point is fixed as the terminal point  $\mathbf{x}_n$ , and the preceding point is determined as

$$\mathbf{x}_m = \mathbf{x}_n, \mathbf{x}_{m-1} = \mathbf{x}_{j'}. \quad (5)$$

Starting from  $(j', n)$  with  $j' = \text{argmax}_j DP(j, n)$ , the remaining points in  $\mathcal{X}'$  are recovered by recursively following the stored predecessor indices.

During navigation, continuous map updates may make the current path no longer collision-free. Upon reaching a segment junction and completing the in-place rotation to align the forward orientation with the next segment, the robot performs *TraversabilityCheck*( $\mathbf{p}_{robot}, \mathbf{p}_{next}, \mathbf{M}$ ), where  $\mathbf{p}_{next}$  is the endpoint of the next line segment. If a predicted collision is detected, global path re-planning is triggered. If no feasible global path can be generated, it indicates that the current target frontier is unreachable. In local frontier point navigation, local exploration will be re-performed. During global frontier point navigation with waypoint retracing, an attempt will be made to skip the current waypoint and plan to the next waypoint. If all waypoints and the selected frontier point are unreachable, local exploration will also be re-performed.

## V. EXPERIMENTS

Figure 8 presents three sets of challenging test scenarios. The first two sets are simulation scenarios with areas of about  $55m^2$  and  $135m^2$ , while the last set a real-world scenario with the area of about  $150m^2$ . Except for the Gazebo simulation running independently on a high-performance workstation, all exploration and mapping calculations are performed on resource-constrained edge computing platform based on Intel N100 (same class as RK3588) and ROS Noetic. A low-cost differential drive robot is used in real-world experiments, and its footprint is simplified to a circumscribed circle with  $r_{robot} = 0.24m$ . It has a 2-D LiDAR with  $r_{sensing} = 20m$ . For mapping, *Cartographer* is used, which is a graph-based SLAM system. To plan and explore on occupancy probability maps it outputs, original maps are ternary processed into traditional occupancy grid maps with three distinct states: unknown, free,

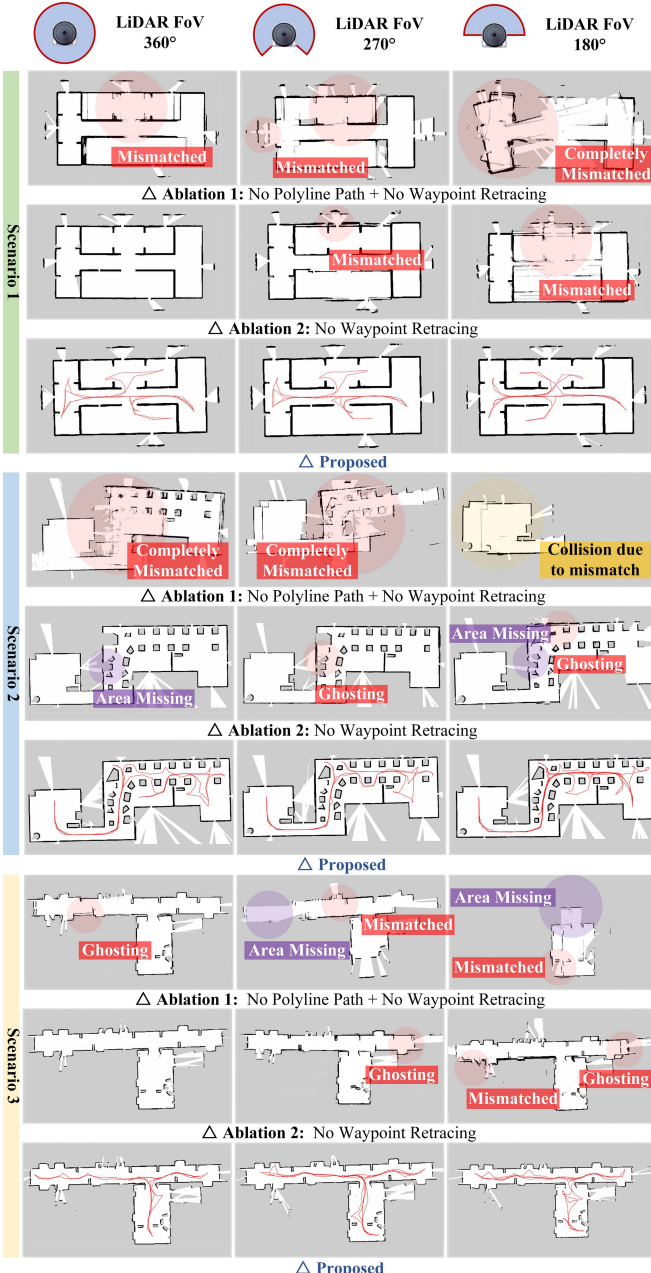


Fig. 9. Partial results of ablation experiments.

and occupied, before being fed into subsequent algorithms. The conducted experiments include: *Case 1*: Polyline path planning experiments. *Case 2*: Exploration-based mapping comparison experiments. *Case 3*: Ablation experiments with multi-FoV configurations. *Case 4*: Mapping time and convergence rate experiments. *Case 5*: Repeated navigation experiments. The demonstration video is at <https://youtu.be/Lw-3I2e544I>.

#### A. Polyline Path Planning Experiments

Since unknown regions are treated as free space in path planning, and the robot remains stationary during polyline path planning based on process design, the effectiveness of polyline path planning can be equivalently validated using fully known maps. The complete maps of scenarios 1 and 2 in Figure 8 are utilized to evaluate the proposed polyline planner, comparing S-Based BI (BI with modified evaluation) and DP-based post-

SCN	Type	FoV (°)	$t_{avg}^{full}$	$t_{avg}^{mapping}$	$N_{sampling\_med}$	$t_{avg}^{sampling}$		$t_{avg}^{retracing}$	CR (%)
						$t_{avg}^{sampling}$	$t_{avg}^{retracing}$		
1	A	M	253.3s	-	-	-	-	-	REF
		360	267.4s	154.2s	3	0.6s	112.6s	96.7	
		270	368.1s	198.6s	3	0.6s	168.9s	96.4	
		180	436.5s	216.8s	4	0.9s	218.8s	96.2	
2	A	M	413.9s	-	-	-	-	-	REF
		360	528.9s	254.0s	7	3.6s	271.3s	99.2	
		270	550.4s	270.6s	8	4.0s	275.8s	98.5	
		180	633.2s	295.6s	10	5.2s	332.4s	97.0	
3	A	M	538.1s	-	-	-	-	-	REF
		360	713.7s	344.6s	4	2.2s	366.9s	98.4	
		270	859.6s	423.4s	5	2.9s	433.3s	98.2	
		180	941.4s	446.1s	6	3.7s	491.6s	96.8	

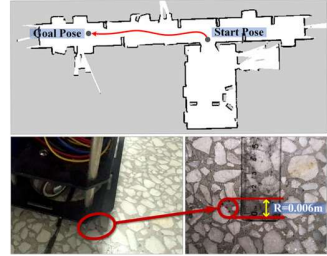


Fig. 10. Results of repeated navigation experiments.

processing. 20 experiments are conducted. Table I presents results for different values of  $d$  ( $d = 1.0$ ,  $d = 1.5$ , and  $d = 2.0$ ), including the pooled STD  $s_p$  of segment lengths, the average cumulative in-place rotation angle  $\varphi_{avg}^{sum}$ , and the average computation time  $t_{avg}^{calc}$  for both methods. Figure 7 further illustrates planned polyline paths of original BI, S-Based BI, and DP. Overall, original BI is unsuitable, while DP achieves more globally optimal solutions but requires higher computation times than S-Based BI. Based on data analysis, both DP and S-Based BI are practical and have similar effects. They will be randomly selected in subsequent experiments. Moreover, to balance efficiency and observation density,  $d$  is set to 1.25.

#### B. Exploration Mapping Comparison Experiments

In these experiments, the proposed algorithm is compared with exploration based on Multiple RRTs (M-RRTs) [8] and Multiple Adaptive RRTs (MA-RRTs), which incorporates the adaptive RRT expansion mechanism from [10] into [8]. The LiDAR FoV is 360°.  $\eta_{max}$  of all methods is set to 0.5m. The proposed framework uses  $c_{RRT} = 0.3m$ , a maximum linear velocity of 1.25m/s, and a maximum angular velocity of 1.57rad/s. M-RRTs and MA-RRTs use a maximum linear velocity of 0.5m/s, roughly equivalent to the average velocity of the proposed framework, and a maximum angular velocity of 1.57rad/s. Each approach is run 20 times in each scenario. Table II presents the number of finishes (FIN), and failures because of collisions (CO) or oscillation-caused deadlocks (OS). The scenarios involve challenges such as ray leakages and constrained areas. For baselines, finish is defined as the map being visually complete. The proposed framework performs better in autonomous mapping tasks in all three scenarios, without collision, oscillation, or deadlock. Figure 8 illustrates sample final maps, showing that MA-RRTs outperformed M-RRTs, while the proposed framework built the most complete, structured, and precise maps.

### C. Ablation Experiments with Multi-FoV Configurations

Ablation experiments evaluate the effectiveness of key components in the proposed framework under different robot LiDAR FoV configurations ( $360^\circ$ ,  $270^\circ$ , and  $180^\circ$ ). Two ablation groups were tested for comparison with the mapping results of the complete proposed framework: *Ablation 1* disables both polyline planner and waypoint retracing, while *Ablation 2* retains polyline planner but disables waypoint retracing. For both the complete framework and the two ablation groups, the relevant parameters were consistent with *Case 2*, and experiments for each group were repeated 20 times. The partial results in Figure 9 illustrate the increasing importance of the stepwise and consistent motion pattern and waypoint retracing mechanism as the LiDAR FoV decreases. Additionally, the proposed framework maintains consistent mapping results under visual observation across various LiDAR FoV configurations.

### D. Mapping Time and Convergence Rate Experiments

This section further analyzes exploration mapping time and coverage based on the 180 trials conducted in *Case 3* across three scene types and three LiDAR FoV configurations. In autonomous exploration-based mapping, the performance of experienced human operators is commonly regarded as a practical baseline, since skilled operators can interpret global scene structure, avoid redundant local searches, and adjust paths strategically to achieve high coverage with relatively low redundancy. As the objective of the proposed framework is to provide reliable mapping on a low-cost platform that can replace manual operation rather than to pursue theoretically minimal exploration time, comparing autonomous results with human performance offers a practical assessment of real-world applicability and substitutability. A similar evaluation methodology can be found in [31], where manually designed trajectories are treated as a high-quality reference for validating the autonomous algorithm.

Table III summarizes the results. Type M denotes the statistics from twenty human-operated trials, whose average covered area serves as the reference coverage rate, and type A denotes the autonomous results.  $t_{avg}^{full}$  represents the average total mapping time, which includes the average base mapping time  $t_{avg}^{mapping}$ , average cumulative local sampling time  $t_{avg}^{sampling}$  and the average waypoint retracing time  $t_{avg}^{retracing}$ .  $N_{med}^{sampling}$  is the median number of local frontier search events over the twenty trials. The results show that across all scene types and LiDAR FoV configurations, the proposed framework achieves more than 96% of the human reference coverage while maintaining a total mapping time only slightly slower than manual operation, remaining within 2min30s. Within the same scene, decreasing the FoV increases  $N_{med}^{sampling}$  and  $t_{avg}^{sampling}$ , yet their influence on the overall mapping time remains limited. This indicates that the proposed SC-RRT continues to efficiently saturate the local reachable space under stationary local frontier search. Coverage also remains stable across different FoV settings, consistent with the observations in *Case 3*, demonstrating robustness to FoV variation.  $t_{avg}^{retracing}$  accounts for nearly half of the total time. Combined with the ablation results in *Case 3*, this confirms that waypoint

retracing is essential for maintaining mapping precision on low-cost platforms and is similarly required during manual operation. It further suggests that on higher-performance hardware where retracing can be reduced or avoided, the proposed framework would offer substantially improved efficiency, as reflected by the relatively small base mapping time  $t_{avg}^{mapping}$ .

### E. Repeated Navigation Experiments

As shown in Figure 10, five repeated navigation trials are conducted on the autonomously constructed map using the path planner from [3] and the motion planner from [2]. The resulting positional error remains within  $\pm 0.006m$ , indicating that the proposed framework generates maps with sufficient precision to support high-precision navigation tasks.

## VI. CONCLUSION

This paper presents a 2-D autonomous collision-free exploration framework for low-cost mobile robots to achieve precise mapping. It is process-complete and can achieve a closed-loop automatic exploration and mapping process. It is suitable for working with modern graph-based SLAM. The enhanced RRT-based frontier search mechanism enables immediate in-situ sampling within a finite timeframe during local exploration, prevents unreachable frontiers in both local and global trees, and reduces potential collisions and deadlocks. The polyline path planner, designed to guide the stepwise and consistent robot motion pattern, improves SLAM mapping precision. The sequential frontier selection and navigation process eliminates oscillations caused by frequent goal pose switching. Additionally, the waypoint retracing mechanism facilitates revisiting previously explored points, promoting loop closure detection and backend optimization in graph-based SLAM. Experiments validate the effectiveness and robustness of the framework across complex environments, low-cost platforms, and LiDAR FoV configurations, achieving an overall exploration success rate exceeding 98%. Compared with experienced human operators, the framework attains more than 96% of the reference coverage within comparable mapping time. Moreover, across the  $360^\circ$ ,  $270^\circ$ , and  $180^\circ$  FoV settings, the variation in the achieved map area remains within 2%.

In the future, we will continue to study the integration of semantic recognition into the mapping process to achieve fully automatic robotic deployment.

## REFERENCES

- [1] M. -A. Chung and C. -W. Lin, "An Improved Localization of Mobile Robotic System Based on AMCL Algorithm," in *IEEE Sensors Journal*, vol. 22, no. 1, pp. 900-908, 1 Jan.1, 2022.
- [2] X. Bu *et al.*, "Path-Follower: A High-Precision Sampling-Based Motion Planner for Inspection Robot," *2023 42nd Chinese Control Conference (CCC)*, Tianjin, China, 2023, pp. 4328-4333.
- [3] Y. Wu *et al.*, "Obstacle-Inflation-Free Global Path Planner for Mobile Inspection Robots in Constrained Industrial Environments," *2024 IEEE 13th Data Driven Control and Learning Systems Conference (DDCLS)*, Kaifeng, China, 2024, pp. 280-285.
- [4] M. Zhang, L. Ma, Y. Wu, K. Shen, Y. Sun and H. Leung, "High-Traversability and Precise Navigation for Mobile Robots in Constrained Environments," in *IEEE Sensors Journal*, vol. 25, no. 12, pp. 22815-22826, 15 June15, 2025.

[5] B. Li, J. Han, Y. Cheng, C. Tan, P. Qi, J. Zhang, and X. Li, "Object goal navigation in embodied AI: A survey," in *Proc. 2022 4th Int. Conf. Video, Signal Image Process. (VSIP)*, Shanghai, China, 2023, pp. 87-92.

[6] J. Sun, J. Wu, Z. Ji and Y. -K. Lai, "A Survey of Object Goal Navigation," in *IEEE Transactions on Automation Science and Engineering*, vol. 22, pp. 2292-2308, 2025.

[7] A. Anwar, J. Welsh, J. Biswas, S. Pouya, and Y. Chang, "ReMEMbR: Building and Reasoning Over Long-Horizon Spatio-Temporal Memory for Robot Navigation," *arXiv preprint arXiv:2409.13682*, 2024. [Online]. Available: <https://arxiv.org/abs/2409.13682>.

[8] H. Umari and S. Mukhopadhyay, "Autonomous robotic exploration based on multiple rapidly-exploring randomized trees," *2017 IEEE/RSJ International Conference on Intelligent Robots and Systems (IROS)*, Vancouver, BC, Canada, 2017, pp. 1396-1402.

[9] D. S. Sundarsingh, J. Bhagiya, J. Chatrola and P. Jagtap, "Autonomous Exploration Using Ground Robots with Safety Guarantees," *2023 IEEE/RSJ International Conference on Intelligent Robots and Systems (IROS)*, Detroit, MI, USA, 2023, pp. 9745-9750.

[10] S. Wu, C. Wang, J. Pan, D. Han and Z. Zhao, "Bayesian-Guided Evolutionary Strategy with RRT for Multi-Robot Exploration," *2024 IEEE International Conference on Robotics and Automation (ICRA)*, Yokohama, Japan, 2024, pp. 12720-12726.

[11] E. Marder Eppstein, *move\_base - ros wiki*, 2016, [online] Available: [http://wiki.ros.org/move\\_base](http://wiki.ros.org/move_base).

[12] Y. Wang, B. Ren, X. Zhang, P. Wang, C. Wang, R. Song, Y. Li, and M. Q.-H. Meng, "ROLO-SLAM: Rotation-Optimized LiDAR-Only SLAM in uneven terrain with ground vehicle," *Journal of Field Robotics*, Wiley Online Library, 2025.

[13] E. B. Olson, "Real-time correlative scan matching," *2009 IEEE International Conference on Robotics and Automation*, Kobe, Japan, 2009, pp. 4387-4393.

[14] W. Hess, D. Kohler, H. Rapp and D. Andor, "Real-time loop closure in 2D LIDAR SLAM," *2016 IEEE International Conference on Robotics and Automation (ICRA)*, Stockholm, Sweden, 2016, pp. 1271-1278.

[15] S. Macenski and I. Jambrecic, "SLAM Toolbox: SLAM for the dynamic world," *Journal of Open Source Software*, vol. 6, no. 61, p. 2783, 2021.

[16] T.-W. Kang, J.-G. Kang, and J.-W. Jung, "A bidirectional interpolation method for post-processing in sampling-based robot path planning," *Sensors*, vol. 21, no. 21, p. 7425, 2021.

[17] Y. Li and H. Cheng, "APP: A\* Post-Processing Algorithm for Robots With Bidirectional Shortcut and Path Perturbation," in *IEEE Robotics and Automation Letters*, vol. 8, no. 11, pp. 7775-7782, Nov. 2023.

[18] B. Yamauchi, "A frontier-based approach for autonomous exploration," *Proceedings 1997 IEEE International Symposium on Computational Intelligence in Robotics and Automation CIRA'97. Towards New Computational Principles for Robotics and Automation'*, Monterey, CA, USA, 1997, pp. 146-151.

[19] B. Fang, J. Ding and Z. Wang, "Autonomous robotic exploration based on frontier point optimization and multistep path planning," in *IEEE Access*, vol. 7, pp. 46104-46113, 2019.

[20] J. Oršulić, D. Miklić and Z. Kovačić, "Efficient Dense Frontier Detection for 2-D Graph SLAM Based on Occupancy Grid Submaps," in *IEEE Robotics and Automation Letters*, vol. 4, no. 4, pp. 3569-3576, Oct. 2019.

[21] H. Zhu, C. Cao, Y. Xia, S. Scherer, J. Zhang and W. Wang, "DSVP: Dual-Stage Viewpoint Planner for Rapid Exploration by Dynamic Expansion," *2021 IEEE/RSJ International Conference on Intelligent Robots and Systems (IROS)*, Prague, Czech Republic, 2021, pp. 7623-7630.

[22] Z. Sun, B. Wu, C. Xu and H. Kong, "Ada-Detector: Adaptive Frontier Detector for Rapid Exploration," *2022 International Conference on Robotics and Automation (ICRA)*, Philadelphia, PA, USA, 2022, pp. 3706-3712.

[23] E. Sumer and H. Temeltas, "RRT Based Frontier Point Detection for 2D Autonomous Exploration," *2022 7th International Conference on Robotics and Automation Engineering (ICRAE)*, Singapore, 2022, pp. 305-311.

[24] D. Zhu, T. Li, D. Ho, C. Wang and M. Q. . -H. Meng, "Deep Reinforcement Learning Supervised Autonomous Exploration in Office Environments," *2018 IEEE International Conference on Robotics and Automation (ICRA)*, Brisbane, QLD, Australia, 2018, pp. 7548-7555.

[25] F. Niroui, K. Zhang, Z. Kashino and G. Nejat, "Deep Reinforcement Learning Robot for Search and Rescue Applications: Exploration in Unknown Cluttered Environments," in *IEEE Robotics and Automation Letters*, vol. 4, no. 2, pp. 610-617, April 2019.

[26] T. Chen, S. Gupta, and A. Gupta, "Learning exploration policies for navigation," *arXiv preprint arXiv:1903.01959*, 2019. [Online]. Available: <https://arxiv.org/abs/1903.01959>.

[27] R. Reinhart, T. Dang, E. Hand, C. Papachristos and K. Alexis, "Learning-based Path Planning for Autonomous Exploration of Subterranean Environments," *2020 IEEE International Conference on Robotics and Automation (ICRA)*, Paris, France, 2020, pp. 1215-1221.

[28] G. Grisetti, C. Stachniss and W. Burgard, "Improved Techniques for Grid Mapping With Rao-Blackwellized Particle Filters," in *IEEE Transactions on Robotics*, vol. 23, no. 1, pp. 34-46, Feb. 2007.

[29] D. H. Douglas and T. K. Peucker, "Algorithms for the reduction of the number of points required to represent a digitized line or its caricature," *CARTOGRAPHICA*, vol. 10, no. 2, pp. 112-122, 1973.

[30] I. A. Sucan, M. Moll and L. E. Kavraki, "The Open Motion Planning Library," in *IEEE Robotics & Automation Magazine*, vol. 19, no. 4, pp. 72-82, Dec. 2012.

[31] Z. Jian, S. Zhang, S. Chen, Z. Nan and N. Zheng, "A Global-Local Coupling Two-Stage Path Planning Method for Mobile Robots," in *IEEE Robotics and Automation Letters*, vol. 6, no. 3, pp. 5349-5356, July 2021.